Ultrafast dynamics of reversible photoinduced phase transitions in rubidium manganese hexacyanoferrate investigated by midinfrared CN vibration spectroscopy

Akifumi Asahara,[1] Makoto Nakajima,[1,*] Ryo Fukaya,[1,†] Hiroko Tokoro,[2] Shin-ichi Ohkoshi,[2] and Tohru Suemoto[1]

[1]*Institute of Solid State Physics, University of Tokyo, 5-1-5 Kashiwanoha, Kashiwa-shi, Chiba 277-8581, Japan*

[2]*Department of Chemistry, School of Science, University of Tokyo, 7-3-1 Hongo, Bunkyo-ku, Tokyo 113-0033, Japan*

(Received 27 April 2012; revised manuscript received 7 November 2012; published 26 November 2012)

Photoinduced phase switching dynamics between LTP (low-temperature phase: Fe^{2+}-CN-Mn^{3+}) and PIHTP (photoinduced high-temperature phase: Fe^{3+}-CN-Mn^{2+}) in rubidium manganese hexacyanoferrate at 4 K was investigated by visible pump midinfrared probe transient absorption spectroscopy. By monitoring the CN stretching vibration modes, which are sensitive to the valence states of the adjacent metal ions, we could qualify not only LTP and PIHTP but also the phase boundary configurations (Fe^{2+}-CN-Mn^{2+} and Fe^{3+}-CN-Mn^{3+}). In addition, by irradiating with another light inducing the reverse process to the pump light, we were able to apply a pump-probe measurement to the persistent phase transitions. The electronic and structural dynamics in the picosecond region were understood with a phenomenological spectral fitting model. In particular, in both directions of these phase transitions, the instantaneous generation of the boundary configuration was observed. This observation suggests that relatively small domains and/or low-dimensional fjord-like domains are created at the early stage of the transition.

DOI: 10.1103/PhysRevB.86.195138 PACS number(s): 78.47.jb, 78.30.−j, 64.60.−i, 82.50.Hp

I. INTRODUCTION

Optical control of physical properties of solids has been attracting much attention of researchers on materials science and technology. Photoinduced phase transition is particularly useful, because drastic changes in electric, dielectric, and magnetic properties are induced, and the changes can be ultrafast or permanent depending on the material. The former will be useful for switching devices and the latter for storage of information. Cyanobridged metal complexes (Prussian blue analogs), which exhibit a variety of optical responses, provide suitable platforms for such investigations.[1–10] In particular, rubidium manganese hexacyanoferrate has been vigorously investigated for its multifunctionality.[11–20] For instance, pressure-induced phase transition,[17] x-ray-induced phase transition,[18] simultaneous occurrence of ferroelectricity and ferromagnetism,[19] and electric-field-induced phase transition[20] have been reported.

Rubidium manganese hexacyanoferrate exhibits a temperature-induced phase transition with a large hysteresis loop between high-temperature phase (HTP) and low-temperature phase (LTP).[21] The size of the hysteresis loop defined by lower and upper phase transition temperatures $T_{1/2\downarrow}$ and $T_{1/2\uparrow}$ strongly depends on the stoichiometry of the sample.[22] The phase transition is triggered by charge transfer between Fe and Mn ions and accompanied by change of the structural and magnetic properties. In HTP, metal ions of Fe^{3+} [$S = 1/2$, low spin (LS)] and Mn^{2+} [$S = 5/2$, high spin (HS)] are bridged by CN^- ligands and construct a three-dimensional lattice, and Rb^+ ions are alternately placed on interstitial sites. The crystal has a cubic structure at room temperature. In LTP, the charge configurations are Fe^{2+} ($S = 0$, LS) and Mn^{3+} ($S = 2$, HS) and the crystal structure is tetragonal, for the lattice is uniaxially distorted by the Jahn-Teller effect at Mn sites. The magnetization changes at $T_{1/2\downarrow}$ or $T_{1/2\uparrow}$ because the total spin changes from $S_{\text{total}} = 3$in HTP to $S_{\text{total}} = 2$ in LTP. LTP shows ferromagnetic ordering under the Curie temperature (12 K).

Recently, it was also reported that a reversible photoinduced phase transition between LTP and a photoinduced high-temperature phase (PIHTP) is repeatedly controlled by irradiating the sample with lights at two different wavelengths, 410 and 532 nm, at 3 K.[23] In PIHTP, the charge configurations are the same as that in HTP, and the crystal has a nearly cubic structure with a slight tetragonal distortion. Since PIHTP has electronic and structural properties similar to those of HTP, we call the photogenerated state at low temperature the PIHTP. It exhibits antiferromagnetic ordering under the Néel temperature (11.5 K).

From the previous ellipsometric study, the process of the phase transition is interpreted as follows.[24] When LTP is irradiated by light at a wavelength of 532 nm, the intervalence transfer (IT) band is excited, and charges at Fe^{2+} are transferred to Mn^{3+} to create PIHTP. In the inverse process, when PIHTP is irradiated by light at a wavelength of 410 nm, the ligand to metal charge transfer (LMCT) band is excited to induce charge transfer from CN^- to Fe^{3+}. Subsequently, charges are supplied from Mn^{2+} to CN, and PIHTP is reversed to LTP.

In this paper, we applied visible pump midinfrared probe transient absorption spectroscopy to investigate the dynamics of the photoinduced phase transitions between LTP and PIHTP. Since the phase transition is triggered by the charge transfer, it is significant to study the picosecond charge dynamics to comprehend the phase transition mechanism in detail. The frequencies of the CN stretching vibration modes in the midinfrared range are very sensitive to the valence states of the adjacent metal ions, and the relations between the resonant frequencies and the valence states have been empirically obtained. Hence, we can utilize the vibration spectroscopy, midinfrared or Raman spectroscopy, as an indicator of the phase transition and quantify the distribution of not only LTP and PIHTP but also boundary configurations (Fe^{2+}-CN-Mn^{2+} and Fe^{3+}-CN-Mn^{3+}), which exist on the boundary of LTP and PIHTP domains.[25] Since the photoinduced phase is persistent, it is normally difficult to apply pump-probe spectroscopy with

 ©2012 American Physical Society

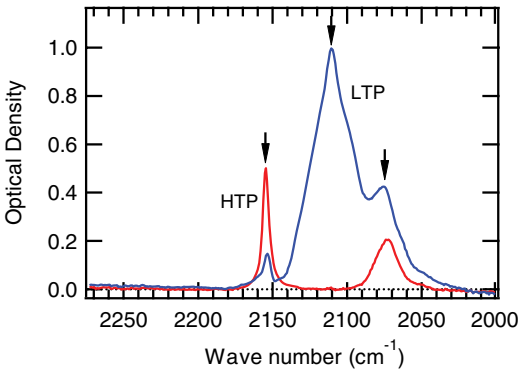

FIG. 1. (Color online) Static absorption spectra of HTP at room temperature (red) and LTP at 4 K (blue).

repeated pumping. However, we enabled the measurement by introducing an accumulation-free method,[26] which is an idea that the initial state for every pump pulse is recovered by irradiating with another light inducing the reverse process.

II. EXPERIMENTAL DETAILS

A. Sample properties

The sample we used was a film with a composition of $Rb_{0.94}Mn[Fe(CN)_6]_{0.98} \cdot 1.3H_2O$ formed on a sapphire substrate.[27] The film consisted of microcrystals with sizes of micrometers, and the thickness is estimated to be about 1 μm. The phase transition temperatures between HTP and LTP in the cooling and warming processes are $T_{1/2\downarrow} = 145$ K and $T_{1/2\uparrow} = 290$ K, respectively. In Fig. 1, we showed the absorption spectrum of HTP at room temperature (RT) and that of LTP generated by cooling the sample to 4 K. The assignments of these peaks were based on empirically obtained relations between CN stretching vibration frequency and the valence states of the adjacent metal ions as discussed in detail by Vertelman *et al.*[28] The frequencies for Fe^{2+}-CN-M^{2+}, Fe^{2+}-CN-M^{3+}, Fe^{3+}-CN-M^{2+}, and Fe^{3+}-CN-M^{3+} (M = transition metal) have been reported to appear in the ranges of 2065–2110, 2090–2140, 2146–2185, and 2180–2200 cm^{-1}, respectively, in infrared and Raman spectroscopy. It is found that the frequencies tend to become higher as the valence numbers of the adjacent metal ions increase. From this empirical law, the sharp peak at 2154 cm^{-1} shown in Fig. 1 is assigned to Fe^{3+}-CN-Mn^{2+} (HTP). The relatively sharp peak at 2074 cm^{-1} in the spectrum of HTP in Fig. 1 can be assigned to Fe^{2+}-CN-Mn^{2+} of $Rb_2Mn[Fe(CN)_6]$, which is slightly included as isolated microcrystallines from the synthesis.[29] Upon cooling, the peak at 2154 cm^{-1} corresponding to HTP gradually decreases around the lower side of the hysteresis loop at 145 K, and the large broad peak at 2110 cm^{-1} arises. This peak is assigned to Fe^{2+}-CN-Mn^{3+} (LTP) from the empirical relation.

B. Experimental setup

We performed visible pump midinfrared probe transient absorption measurement to investigate the picosecond charge-transfer dynamics of the reversible phase transition processes, LTP to PIHTP and PIHTP to LTP, in rubidium manganese hexacyanoferrate. The sample was mounted in a cryostat equipped with CaF_2 windows, and all the measurements were carried out at 4 K.

We employed a 1 kHz repetitive regenerative amplifier system (Spectra Physics, Spitfire) producing 120 fs pulses at 800 nm seeded by a mode-locked Ti:sapphire laser (Spectra Physics, TSUNAMI 3160C), and the output was divided into pump and probe beams. The pump beam was mechanically chopped at 500 Hz for lock-in detection. In investigating LTP to PIHTP conversion, pump pulses at a wavelength of 532 nm, which resonantly excite the IT band to induce the charge transfer from Fe^{2+} to Mn^{3+}, were generated by taking sum frequency of the fundamental beam and the idler beam from an optical parametric amplifier (OPA) (Light Conversion, TOPAS-C) with a nonlinear optical crystal, β-BaB_2O_4 (BBO). On the other hand, to investigate the reverse process, PIHTP to LTP conversion, we excited the LMCT band to induce charge transfer from Mn^{3+} to Fe^{2+}. We generated second harmonics of the fundamental wave at 400 nm with a BBO crystal and employed it as pump pulses. The probe pulses in the midinfrared region monitoring CN stretching vibration modes were generated by taking the difference frequency of signal and idler beams from another OPA system (Light Conversion, TOPAS-C). The probe light transmitted through the sample was monochromatized by a grating monochromator (Nikon, G250) and was detected by an InSb photoconductive detector. The wave number resolution in our measurement condition is about 2 cm^{-1}. Two lock-in amplifiers which were synchronized to 1 kHz and 500 Hz, respectively, were used to record the intensity of the transmitted light and the transient absorption change simultaneously. The time resolution of this measurement system is approximately 260 fs, which was estimated by measuring cross-correlation of the pump and probe pulses.

In these experiments, beams inducing the inverse processes were simultaneously directed to the sample to suppress accumulating of the photoinduced phase during measurements, which we call the accumulation-free method.[26] When we irradiated the sample with the pump beam at a wavelength of 532 nm, a quasicontinuous wave (CW) light at a wavelength of 400 nm was simultaneously directed to the sample. The quasi-CW light was obtained by generating second harmonics of another mode-locked Ti:sapphire oscillator (Spectra Physics, TSUNAMI 3950C) producing 1.5 ps pulses at a wavelength of 800 nm. Since the repetition rate of 82 MHz is sufficiently high, we regard it as a quasi-CW light source. On the other hand, when we pumped the sample with the beam at a wavelength of 400 nm, a CW light at a wavelength of 532 nm was simultaneously directed to the sample. The CW light was obtained from a frequency-doubled yttrium aluminum garnet laser pumped by a diode laser. If the CW light is not irradiated, the photoinduced phase becomes dominant within a few minutes.[26] Although the accumulation of the photoinduced phase is not completely removed, in this way we could keep the photoinduced phases at low concentrations for a long time required for pump-probe measurement. The transient signal is not affected by the CW light itself, because its fluence in the time scale observed in our experiment (several hundreds of picoseconds) is negligibly small compared to that of the pump light.

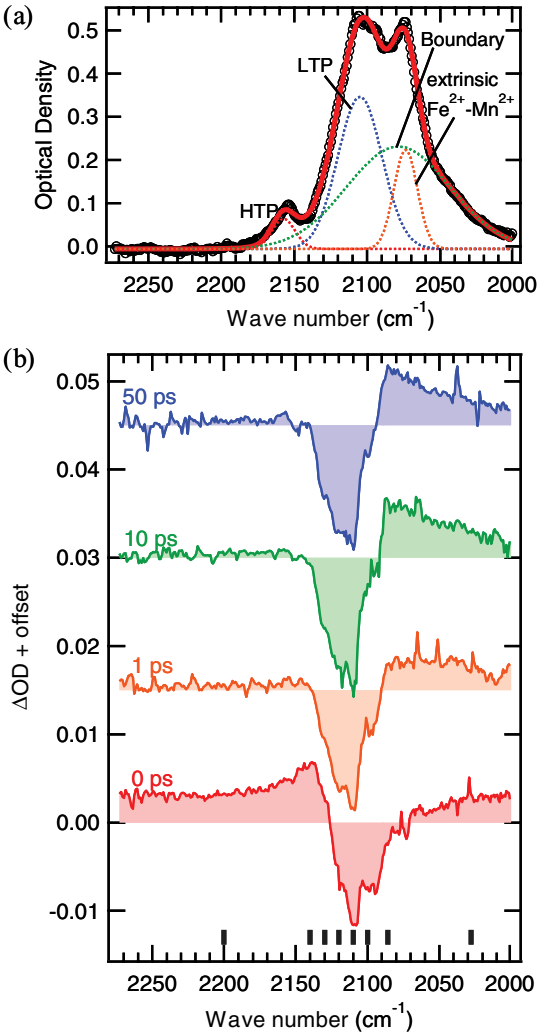

FIG. 2. (Color online) (a) Static absorption spectrum of LTP during the experiment observing the dynamics of the phase transition from LTP to PIHTP (black circle) and the fitting result (red solid line). The decomposed four components, HTP (red), LTP (blue), boundary (green), and extrinsic Fe^{2+}-Mn^{2+} (orange), are also exhibited as dotted lines. (b) Transient absorption spectra at 0, 1, 10, and 50 ps showing the dynamics of the phase transition from LTP to PIHTP. The excitation density of pump pulses and CW light are 0.4 W/cm^2 and 2 W/cm^2, respectively.

III. RESULTS AND DISCUSSION

A. LTP to PIHTP transition

To observe the dynamics of the LTP to PIHTP transition, we performed transient midinfrared absorption measurement with pump pulses at a wavelength of 532 nm (0.4 W/cm^2). Quasi-CW light at a wavelength of 400 nm (2 W/cm^2) simultaneously irradiates the sample to keep the concentration of the PIHTP at a low level during the measurement. Figure 2(a) shows the absorption spectrum at 4 K during the measurement. The experimental data are expressed as black circles without smoothing process. It is found that the spectrum has some differences from the original LTP spectrum in Fig. 1. The main changes are the decrease of the peak at 2105 cm^{-1} corresponding to LTP and the increase of the magnitude around 2080 cm^{-1}. To investigate the spectrum in detail, we tried to decompose it into four components containing LTP mentioned above by a least-squares fitting method. The same fitting processes are applied in the analyses described later. Here we assumed Gaussian functions for the spectral components, because the broadenings of these peaks are ascribed to the randomness of the environment, which is caused by random lattice strains of various magnitudes in various directions. From the comparison with the spectrum in Fig. 1, the small peak at 2157 cm^{-1} is ascribed to HTP. The relatively sharp peak at 2074 cm^{-1} is assigned to Fe^{2+}-CN-Mn^{2+} valence configuration of $Rb_2Mn[Fe(CN)_6]$ as mentioned in the previous section. Since this component is assigned to isolated $Rb_2Mn[Fe(CN)_6]$ particles and will not contribute to the concerned phase transition process, we call it "extrinsic Fe^{2+}-Mn^{2+}" and neglect it in the discussions hereafter. Assignment of the broad peak at around 2079 cm^{-1} is not straightforward, because this component is hardly observed in HTP at RT or in fresh LTP generated by cooling shown in Fig. 1. It gradually arises when 532 nm pump pulses and 400 nm CW laser light, which induce the inverse phase transitions, simultaneously irradiate the sample. Since the center wavelength of this peak is located in the typical frequency range corresponding to Fe^{2+}-CN-Mn^{2+} (2065–2110 cm^{-1}), it can be assigned to this valence configuration. Although the low-frequency tail of this band exceeds the typical range, it is also ascribed to Fe^{2+}-CN-Mn^{2+}, because only the low valence pair can appear in the low-frequency region. We call this component the "boundary" in the following discussions, because it appears only on the boundary between LTP and PIHTP as mentioned in the first section of this paper. It is interpreted that such a large number of the boundary configurations arise because the PIHTP domains are fragmented into small clusters while repeating the innumerable phase switching processes. Once this broad peak due to the boundary is created, it hardly decreases even if we stop the pump pulses keeping irradiation with 400 nm light. We speculate that this fact is explained by the blocking effect whose mechanism has been understood as follows.[25] When $[Fe(CN)_6]^{4-}$ surrounded by six Mn^{2+} ions are congregated to constitute Fe^{2+}-CN-Mn^{2+} clusters, the metal-ion pairs in these clusters become unable to contribute to the charge transfer. Therefore, the number of Fe^{2+}-CN-Mn^{2+} valence pairs does not decrease under irradiation of either 532 nm or 400 nm light. The considerable broadening of this peak is probably caused by random local strain fields which are created on the interface between domains having different lattice constants.

Transient absorption spectra at various delay times in Fig. 2(b) were obtained by scanning the monochromator at fixed delay times. Here, the transmitted light intensity was recorded with the lock-in amplifier synchronized to 1 kHz, and the transient change of the intensity was simultaneously recorded with another lock-in amplifier synchronized to 500 Hz. We calculated the changes of the optical density (OD) with the outputs obtained from these two lock-in amplifiers. We regarded the spiky structures found in Fig. 2(b) as noise and neglected them in the analysis performed later. We show major features read from these spectra as follows. First, decreasing of the absorption around 2110 cm^{-1} due to LTP was found. On the other hand, increasing of the absorption in the lower wave

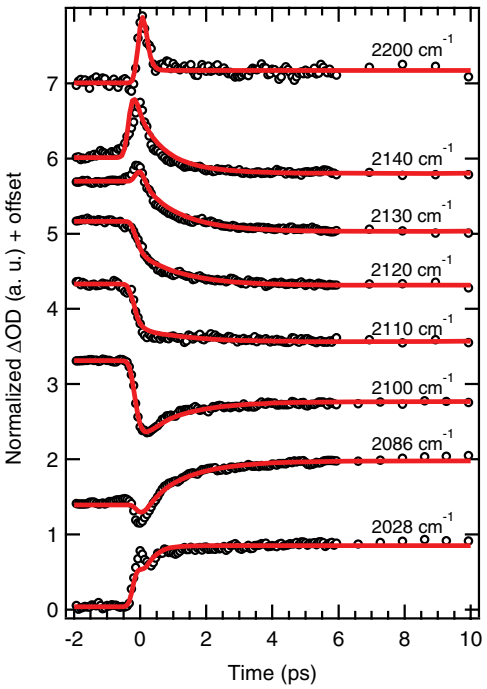

FIG. 3. (Color online) Time evolution curves of normalized transient absorption showing the dynamics of the phase transition from LTP to PIHTP (black circle). The indicated wave numbers correspond to the black rectangles, where the time evolutions were measured, shown at the bottom of Fig. 2. The phenomenological fitting results are inserted as red solid lines.

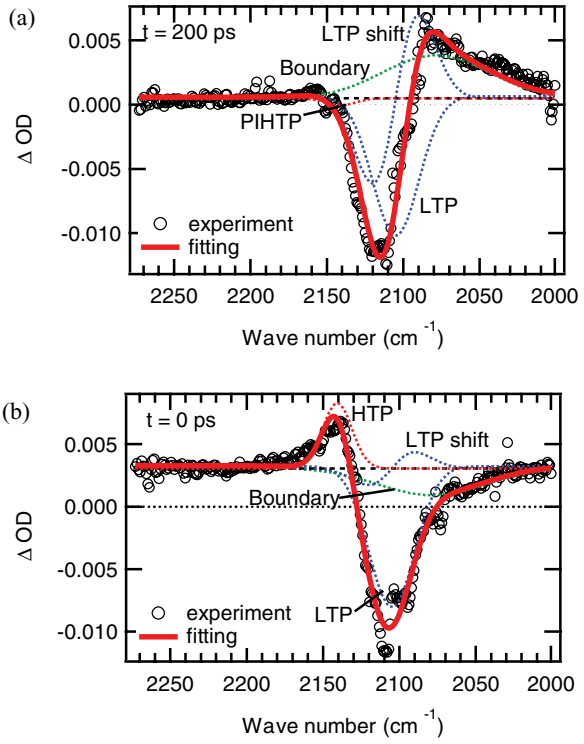

FIG. 4. (Color online) Transient absorption spectra at (a) 200 ps and (b) 0 ps (black circle). The fitting results are inserted as red solid lines, and the decomposed components are exhibited as dotted lines.

number range corresponding to Fe^{2+}-CN-Mn^{2+} (boundary) was also found. We can see also some complicated behaviors in the spectra. At 0 ps, a plateau appears in the higher wave number range, and a bump structure is found around 2140 cm^{-1}. By comparing the spectra at 0 ps and 1 ps, we can find a slight blueshift of the dip around 2110 cm^{-1} and a gradual increase around 2090 cm^{-1}. The complexity was also reflected in the time evolution of normalized transient absorption shown in Fig. 3. These curves were recorded by scanning delay times with the monochromator fixed. These time evolution curves change critically depending on the probe wave number. From this fact, these curves seem to be intermingled by several contributions with different rising and relaxation times. To understand the phenomenon, we tried to decompose the spectra.

Figure 4(a) shows the result of the fitting analysis of the transient absorption spectrum at 200 ps after excitation. We tried to reproduce the spectrum by superposing the following three components defined in Fig. 2(a), i.e., the LTP peak at 2105 cm^{-1}, the boundary peak at 2074 cm^{-1}, and the redshift of the LTP peak, which is expressed as the differentiated wave form of the LTP absorption peak. Here, we considered also a Gaussian component corresponding to PIHTP at 2141 cm^{-1} and a flat offset component. However, the contributions of these two components are found to be negligibly small at 200 ps. These components are necessary at $t = 0$ as discussed in the next paragraph. The large decrease of LTP and the increase of boundary, are interpreted as the reduction of LTP and the production of boundary, respectively, resulting from the charge transfer from Fe^{2+} to Mn^{3+}. The third component, the peak shift of the LTP peak, is ascribed to local strains induced by a lattice mismatch, which arises when the cubic-like PIHTP domain is optically generated in the tetragonal background of LTP. By performing this fitting procedure, the experimental spectrum could be successfully reproduced as expressed by the red solid curve in Fig. 4(a). Here, the experimental spectrum at 200 ps seems to have a small splitting around 2115 cm^{-1}. As the crystal structure in LTP is tetragonal, the LTP component may split into several components. However, since all the components observed in this wave number range (2090–2140 cm^{-1}) can be assigned to the LTP, we neglected this splitting and treated these peaks as one LTP component in the analysis. Here, it is interesting to note that the increase of the PIHTP peak is practically zero, against our natural expectation. This can be understood from two facts. First, the oscillator strength of the PIHTP peak is much smaller than those of LTP and the boundary peaks as found from Fig. 1.[22] Second, the number of newly created PIHTPs accompanying a photoinduced charge transfer is smaller than those of bleached LTPs and generated boundary configurations. As explained in Fig. 5, when a charge transfer occurs at one site in LTPs (Fe^{2+}-CN-Mn^{3+}), only one PIHTP (Fe^{3+}-CN-Mn^{2+}) is newly created at this site, while LTP is bleached at the surrounding 11 sites and boundary configurations (Fe^{2+}-CN-Mn^{2+} and Fe^{3+}-CN-Mn^{3+}) are generated at 10 sites. Incidentally, from the fact that the sizes of the former two changes, i.e., the decrease of the LTP peak and the increase of the boundary peak, are roughly of the same order, it is suggested that the numbers of the disappeared LTPs and the created boundary configurations are also of the same order, provided the oscillator strengths of these peaks are not so different. In the

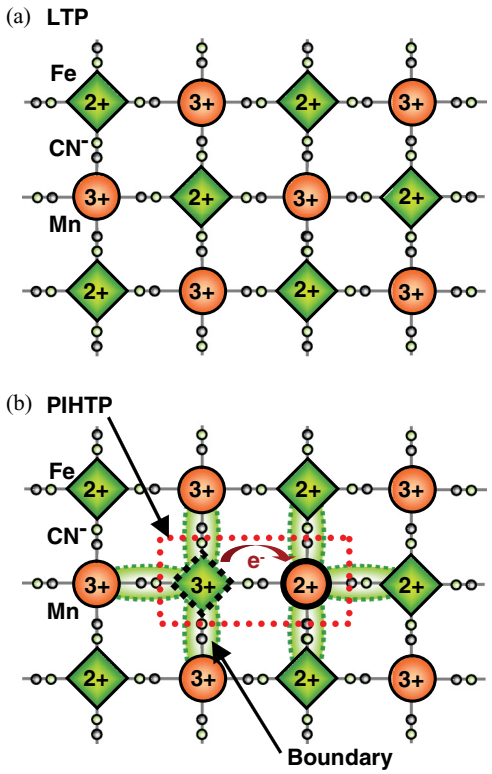

FIG. 5. (Color online) The cross-section of the lattice of $RbMn[Fe(CN)_6]$, where the interstitial Rb^+ ions are omitted for simplification. (a) The distribution of the metal ion's valence numbers in LTP (Fe^{2+}-CN-Mn^{3+}) and (b) that in the situation after one electron is transferred from Fe^{2+} to Mn^{3+}. The charge-transferred site enclosed by the red dotted rectangle is converted to the PIHTP (Fe^{3+}-CN-Mn^{2+}) configuration. At the same time, the CN^- sites masked by green dotted ovals (totally 10 sites) surrounding the charge-transferred site become the boundary configurations (Fe^{2+}-CN-Mn^{2+} or Fe^{3+}-CN-Mn^{3+}).

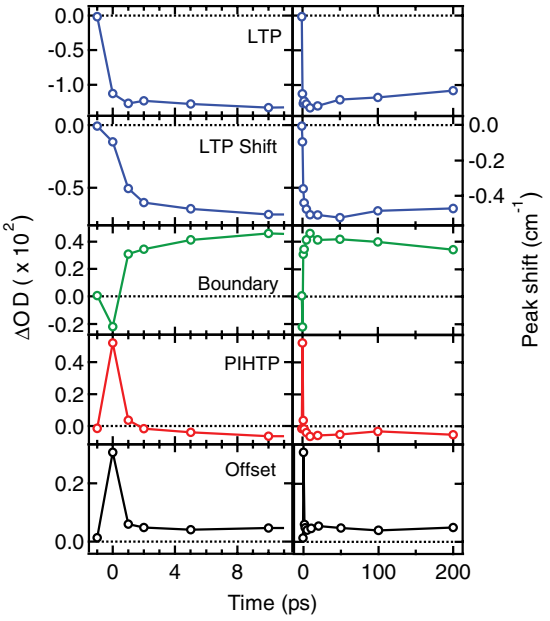

FIG. 6. (Color online) Time evolution curves of the decomposed five components, LTP, the shift of LTP, boundary, PIHTP, and the offset component. The horizontal dotted lines represent zero. The ΔOD values for LTP, boundary, and PIHTP were obtained at the peaks of the Gaussian functions. That for the LTP shift was evaluated at the extremum of the differentiated wave form (2120.5 cm^{-1}). For the plot of LTP shift, the corresponding peak shift is displayed on the right axis.

case of photoinduced phase transition, many initial nuclei are created at random in the LTP background, when photons are absorbed at Fe^{2+}-CN-Mn^{3+} pairs. Consequently, the averaged domain size becomes smaller and/or the domain is apt to have a low-dimensional fjord-like structure.[30] Hence, the relative amount of the boundary configuration is larger than that in the case of thermal phase transition, where the continuous domain growth is the main process of the phase transition.

We applied this decomposition procedure to the transient absorption spectrum at 0 ps with the same components, and we show the results in Fig. 4(b). The significant difference from the spectrum at 200 ps is the positive offset component observed in an extremely wide wave number range. This component is reflected in the time evolution curve at 2200 cm^{-1} in Fig. 3 as a sharp spike at 0 ps. It is found that both its rising and relaxing times are as fast as the time resolution of the measurement system. In addition, we found that the intensity of this component is rather sensitive to the measurement conditions. From these facts, we speculated that the offset component may be due to some nonlinear optical response such as the Kerr-lens effect which is not directly related to the phase transition. Hence, we treated it as a flat component. Removing it from the spectrum, the dominant component is the large decrease of the LTP peak at 2105 cm^{-1}. This spectrum at 0 ps seems to have a double-peaked structure around 2105 cm^{-1}, which might correspond to the structure of the LTP peak shown in Fig. 2(a). This structure in Fig. 2(a) is not clear because the splitting is smaller than the broadening, and several peaks may be overlapping. Here, from the same reason as in the case of Fig. 4(a), we neglected this splitting and regarded it as one LTP component in the analysis. In the spectrum in Fig. 4(b), relatively small decreasings of the boundary peak and the LTP peak shift are also observed. In addition, it is necessary to assume a positive peak at 2141 cm^{-1} to reproduce the bump structure in the experimental spectrum. This component is tentatively assigned to instantaneous PIHTP generation, although the center wave number is slightly lower than that obtained in the static absorption spectrum. This component may correspond to some intermediate state, which is similar to HTP but has somewhat different lattice relaxation.

We decomposed the transient absorption spectra at other delay times from −1 to 200 ps in the same way. Figure 6 summarizes the time evolution of the decomposed five components, i.e., the LTP peak at 2105 cm^{-1}, the shift of LTP peak, the boundary peak at 2079 cm^{-1}, the HTP peak at 2141 cm^{-1}, and the flat offset component. From this analysis, the overall behavior of time evolutions of every component was revealed. The LTP component is instantaneously bleached after the light excitation. The LTP peak shows a redshift of about 0.52 cm^{-1} taking about 1 ps. The boundary component has an irregular behavior in which the absorption decreases at 0 ps and it turns to an increase after 1 ps. These three changes decay slowly and survive longer than 100 ps. PIHTP and the offset component

TABLE I. Function forms and time constants of the components used in the fitting procedure shown in Fig. 3.

i	Component	$I_i(t)$	τ_r(ps) (rising time)	τ_d(ps) (decay time)
1	LTP	$1-\exp(-t/\tau_r)$	0.16	
2	LTP shift	$1-\exp(-t/\tau_r)$	1.32	
3	Boundary	$\exp(-t/\tau_d)$		0.27
		$1-\exp(-t/\tau_r)$	0.31	
4	PIHTP	$\exp(-t/\tau_d)$		0.59
5	Offset	$\exp(-t/\tau_d)$		0.10

rise steeply at the time origin and rapidly relax to the initial state within 1 ps.

In order to analyze more accurately the time evolution at the early stage (<10 ps) of the transition, we tried to reproduce all the experimental time evolution curves shown in Fig. 3 based on these five components. The fitting function is defined as

$$g(t,\omega) = \int f_{\text{inst}}(\tau) \sum_i I_i(t-\tau) C_i(\omega) d\tau \quad (i = 1, 2\ldots,5), \tag{1}$$

where $C_i(\omega)$ is the spectral shape of every component deduced by the decomposition procedure mentioned above, $I_i(t)$ denotes the time evolution curve of every component, and $f_{\text{inst}}(\tau)$ is the instrumental Gaussian function. The subscripts i indicate the spectrum components. As for the spectrum shapes, $C_i(\omega)$, the components of LTP, boundary, and PIHTP ($i = 1$, 3, and 4) are Gaussian functions. The component of the LTP shift ($i = 2$) is the derivative of a Gaussian function, and the offset component ($i = 5$) is a constant independent of wave numbers. The function forms of $I_i(t)$ are defined as shown in Table I to reproduce the shape of the time evolution curves in Fig. 3. In order to describe the irregular shape of the boundary component ($i = 3$), we assumed a sum of two components: One component instantaneously decreases and rapidly relaxes. The other component slowly rises and stays constant. The fitting results are shown in Fig. 3 as red solid curves, and the obtained time constants are summarized in Table I. The fitting curves in Fig. 3 have some deviations from the experimental curves (black circles) around 0 ps. This discrepancy is ascribed to the nonlinear optical response which strongly depends on the measurement conditions as mentioned above. Except for this ambiguity near the time origin, the detailed structures of the experimental curves are well reproduced over the measured wave number range. Since the calculated curves are generally in good agreement with the experimental data, this phenomenological analysis can be justified.

From this analysis, the following scenario is derived. First, light irradiation at 532 nm excites the IT band and induces immediate charge transfer from Fe^{2+} to Mn^{3+}, which is evidenced by a sharp decrease of the LTP band. At the same time, PIHTP is produced at the charge-transferred sites. However, almost all the created PIHTP disappears within 1 ps. Against our natural expectation, the boundary configuration temporarily decreases just after excitation. These behaviors can be understood as follows. When a charge is transferred from Fe^{2+} to Mn^{3+}, Fe^{2+}-CN-Mn^{2+} pairs around this Fe^{2+} disappear and new Fe^{2+}-CN-Mn^{2+} pairs appear around the Mn^{2+}. If the boundary components, i.e., Fe^{2+}-CN-Mn^{2+} and Fe^{3+}-CN-Mn^{3+} pairs, prevails, the number of newly created Fe^{2+}-CN-Mn^{2+} pairs could be smaller than the number of those disappeared, and the net change of boundary component can be negative. If the transient charge-transferred state created in such a "boundary-rich" area is unstable, the momentary decrease of the boundary and the increase of the PIHTP can be understood. After this transient response within one picosecond, the boundary configuration increases in accordance with the decrease of LTP configuration till 10 ps and starts to decrease slowly after that. The existence of a slowly rising component indicates that the change of the phase has some delay from the charge transfer transition itself. The relatively large response of the boundary component indicates that a large number of boundary configurations are created at the charge-transferred site surrounded by the background of the LTP as depicted in Fig. 5(b). Lastly, the LTP peak shift has a rising time of approximately 1 ps, which is clearly slower than the charge-transfer process mentioned above. It can be attributed to a delayed local deformation caused by the dissolution of Jahn-Teller distortion. The time constant 1 ps may correspond to the time required for the lattice to deform. All these photoinduced species except for the short-lived PIHTP survive longer than 100 ps.

B. PIHTP to LTP transition

To observe the dynamics of the PIHTP to LTP transition, we performed transient midinfrared absorption measurement with pump pulses at a wavelength of 400 nm (0.25 W/cm^2). The PIHTP was prepared by irradiating the sample in LTP with the CW light at a wavelength of 532 nm (1 W/cm^2) at 4 K. Irradiation at this wavelength keeps the LTP at low concentration during the pump-probe measurement. The absorption spectrum of PIHTP during the measurement is shown in Fig. 7(a). The spectrum can be reproduced by the four Gaussian functions in the same way mentioned in the previous section. The peaks at 2155, 2099, 2072, and 2074 cm^{-1} are assigned to PIHTP, LTP, boundary, and extrinsic Fe^{2+}-Mn^{2+} of isolated $Rb_2Mn[Fe(CN)_6]$ microcrystals, respectively. The spectral shape is different from that of HTP in Fig. 1 in the point that the HTP peak is smaller and the boundary peak appears. The production of a large size of the boundary component indicates that the size of the photocreated domain is small as in the case of LTP to PIHTP transition discussed in the previous section. Although a small fraction of the LTP component remains, the transient variation observed here mainly reflects the phase transition from PIHTP to LTP, because the number of PIHTPs is sufficiently larger than that of LTPs. The slight differences of the center wave numbers of the peaks between PIHTP in Fig. 7(a) and LTP in Fig. 2(a) are attributed to the strain caused by transformations of the majority crystal structures.

Figure 7(b) shows transient absorption spectra at various delay times in the transition from PIHTP to LTP. We regarded the spiky structures found in these spectra as noise and neglected them in the analysis. The major features of these spectra are described as following. An intense bipolar signal

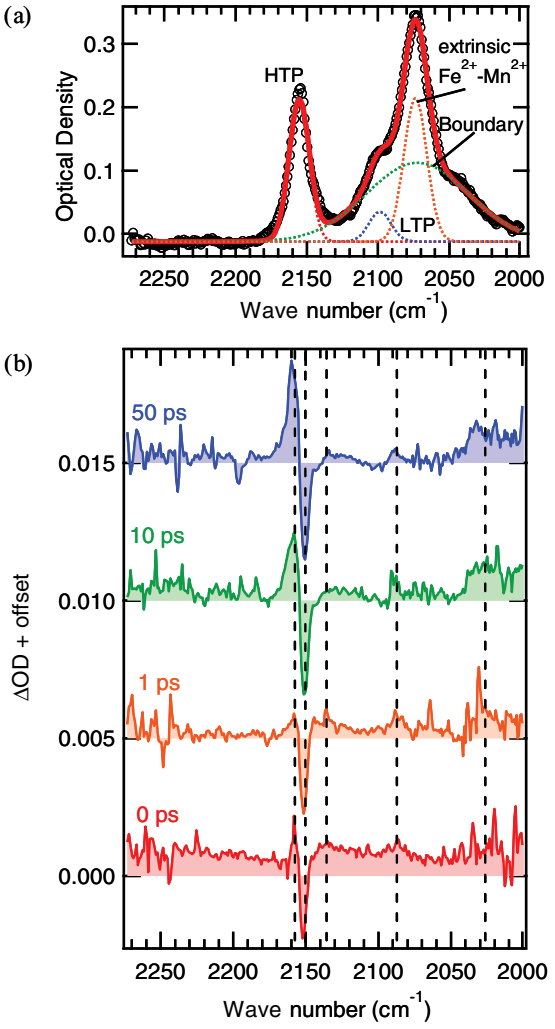

FIG. 7. (Color online) (a) Static absorption spectrum of PIHTP during the experiment observing the dynamics of the phase transition from PIHTP to LTP (black circle) and the fitting result (red solid line). The decomposed four components, HTP (red), LTP (blue), boundary (green), and extrinsic Fe^{2+}-Mn^{2+} (orange), are also exhibited as dotted lines. (b) Transient absorption spectra at 0, 1, 10, and 50 ps showing the dynamics of the phase transition from PIHTP to LTP. The excitation density of pump pulses and CW light are 0.25 W/cm^2 and 1 W/cm^2, respectively.

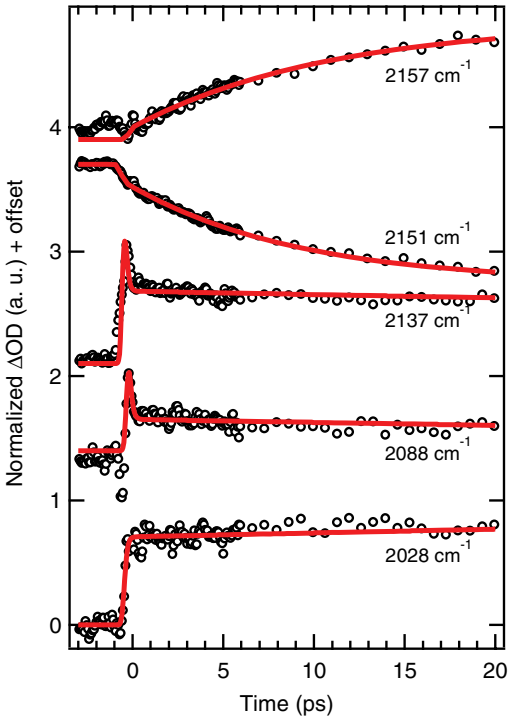

FIG. 8. (Color online) Time evolution curves of normalized transient absorption for the phase transition from PIHTP to LTP at some wave numbers (black circle). The fitting results are inserted as red solid lines.

appears around 2155 cm^{-1}, corresponding to the center wave number of the PIHTP absorption peak. Small peaks can be found around 2000–2140 cm^{-1}. Here, we measured the time evolutions at five wave numbers shown by vertical dashed lines in Fig. 7(b). First, we note the intense positive and negative signals around 2155 cm^{-1}. Since the spectral shape around the wave number is similar to the derivative of the PIHTP absorption band, the signal is assigned to a blueshift of the PIHTP peak. We can estimate that the bipolar signal at 50 ps in Fig. 7(b) corresponds to a blueshift of about 0.20 cm^{-1}. In Fig. 8, the time evolutions at 2157 and 2151 cm^{-1} corresponding to the positive and negative components due to the blueshift, respectively, have rising time constants of about 20 ps. These signals last longer than 100 ps as found by other long scan measurement. Since the response time is a typical value widely found in photoinduced phase transitions,[31] we attributed the shift to local lattice deformation caused by laser-induced local heating. In similar research investigating the transition dynamics from HTP to PILTP at RT,[32] the peak due to HTP was shifted in the inverse direction. This observation can be explained by the temperature dependence of the peak frequency. In lowering the temperature from RT, the peak frequency gradually increases above around 200 K then turns to a decrease.[22] This correspondence further supports the assignment. It is hard to see the net charge of the PIHTP peak, because of the overlapped large signal due to the peak shift.

Second, a broad positive signal is seen around 2028 cm^{-1} in Fig. 7(b). The component can be assigned to production of boundary configurations, because in this low-frequency region the only possible combination of the valence numbers is the lowest valence pair Fe^{2+}-CN-Mn^{2+}. From Fig. 8, it is found that the component rises within the time resolution and survives longer than 100 ps. This means that the instantaneous charge transfer from Mn^{2+} to Fe^{3+} induces the boundary configuration at the same time, which persists longer than 100 ps. In addition, two small positive signals at 2137 and 2088 cm^{-1} are also found in Fig. 7(b). These two features are tentatively ascribed to productions of LTP and/or boundary from the empirical law mentioned before, although the resonance wave numbers are slightly different. The reason for the wave number shifts can be explained as follows. At the early stage of the phase transition from HTP to LTP, such shifts of about 10 cm^{-1} are commonly observed.[24] It has been shown that the shifts are caused by local strains due to a lattice mismatch when the tetragonal LTP domain is optically generated in the background of nearly cubic PIHTP.

The corresponding time evolution curves shown in Fig. 8 can be reproduced by the following two components. One has a spiked shape with a time width the same as the pump pulse. It is tentatively assigned to a nonlinear effect such as the Kerr-lens effect mentioned in the previous section, and is not related to the phase transition. The other has a steplike response and survives longer than 100 ps. It corresponds to instantaneous creations of LTP and/or boundary configurations caused by the photoinduced charge transfer from Mn^{2+} to Fe^{3+}. The origin of this steplike component is probably the same as the signal observed around 2028 cm^{-1} mentioned above.

The scenario of the transition from PIHTP to LTP is summarized as follows. When pump light irradiates the sample, charges on Mn^{2+} sites are transferred to Fe^{3+} in a very short time (within the time resolution of 260 fs) in spite of the two-step charge-transfer processes. At the same time, LTP and boundary configurations are generated and survive longer than 100 ps. In addition, the system is locally heated within approximately 20 ps, and local lattice deformation arises.

IV. CONCLUSION

Transient photoinduced phase transition dynamics initiated by photoinduced charge transfer in rubidium manganese hexacyanoferrate at low temperature was investigated by visible pump midinfrared probe spectroscopy monitoring CN vibration modes. We successfully observed the transient optical responses by applying an accumulation-free method to avoid the effect of overlapped persistent phase transition. This method can be applied to other systems which show persistent phase change, provided the phase can be reversed by irradiating at different wavelengths.

The transient behavior of the CN vibration spectra associated with these photoinduced phase transitions was understood in terms of the phenomenological model. In the transition from LTP to PIHTP induced by the charge transfer from Fe^{2+} to Mn^{3+}, LTP is reduced within the time resolution. Most of the created PIHTP disappears within 1 ps in the "boundary-rich" region. After 1 ps, the boundary configuration increases in accordance with the further decrease of the LTP configuration. The local lattice deformation by the dissolution of the Jahn-Teller distortion takes about 1 ps. The boundary and LTP decay slowly and survive longer than 100 ps. In other words, they are metastable and not persistent. In the transition from PIHTP to LTP, LTP and the boundary configuration are transiently created within the time resolution and show also slow decay. The local heating of the lattice takes about 20 ps.

Here, it is noteworthy that the significant generation of the boundary was observed in both directions of these phase transitions. This suggests that relatively small domains and/or low-dimensional fjord-like domains are created at the early stage of the transition. In conclusion, we have presented an example of boundary-sensitive ultrafast spectroscopy probing transient domain creation.

ACKNOWLEDGMENTS

This work was supported by a Grant-in-Aid for Scientific Research (B) from the Ministry of Education, Culture, Sports, Science, and Technology of Japan, and A.A. was supported by the Global COE Program "The Physical Sciences Frontier," MEXT, Japan.

*Present address: Graduate School of Science, Chiba University, 1-33 Yayoi-cho, Inage-ku, Chiba-shi, Chiba 263-8522, Japan.

†Present address: Department of Chemistry and Materials Science, Tokyo Institute of Technology, 2-12-1 Ookayama, Meguro-ku, Tokyo 152-8551, Japan.

[1] S. Ohkoshi, K. Imoto, Y. Tsunobuchi, S. Takano, and H. Tokoro, Nat. Chem. **3**, 564 (2011).

[2] H. Tokoro and S. Ohkoshi, Dalton Trans. **40**, 6825 (2011).

[3] O. Sato, T. Iyoda, A. Fujishima, and K. Hashimoto, Science **272**, 704 (1996).

[4] O. Sato, Y. Einaga, T. Iyoda, A. Fujishima, and K. Hashimoto, J. Electrochem. Soc. **144**, L11 (1997).

[5] S. Ohkoshi, H. Tokoro, T. Hozumi, Y. Zhang, K. Hashimoto, C. Mathonière, I. Bord, G. Rombaut, M. Vereist, C. Cartier dit Moulin, and F. Villain, J. Am. Chem. Soc. **128**, 270 (2006).

[6] F. Tuna, S. Golhen, L. Ouahab, and J.-P. Sutter, C. R. Chimie **6**, 377 (2003).

[7] S. Ohkoshi, Y. Hamada, T. Matsuda, Y. Tsunobuchi, and H. Tokoro, Chem. Mater. **20**, 3048 (2008).

[8] K. D. Bozdag, J. W. Yoo, N. P. Raju, A. C. McConnell, J. S. Miller, and A. J. Epstein, Phys. Rev. B **82**, 094449 (2010).

[9] H. Kamioka, Y. Moritomo, W. Kosaka, and S. Ohkoshi, Phys. Rev. B **77**, 180301 (2008).

[10] H. Kamioka, Y. Moritomo, W. Kosaka, and S. Ohkoshi, J. Phys. Soc. Jpn. **77**, 093710 (2008).

[11] Y. Moritomo, K. Kato, A. Kuriki, M. Tanaka, M. Sakata, H. Tokoro, S. Ohkoshi, and K. Hashimoto, J. Phys. Soc. Jpn. **71**, 2078 (2002).

[12] A. Ántal, A. Jánossy, L. Forró, E. J. M. Vertelman, P. J. van Koningsbruggen, and P. H. M. van Loosdrecht, Phys. Rev. B **82**, 014422 (2010).

[13] J. Luzon, M. Castro, E. J. M. Vertelman, R. Y. N. Gengler, P. J. van Koningsbruggen, O. Molodtsova, M. Knupfer, P. Rudolf, P. H. M. van Loosdrecht, and R. Broer, J. Phys. Chem. A **112**, 5742 (2008).

[14] T. T. A. Lummen, R. Y. N. Gengler, P. Rudolf, F. Lusitani, E. J. M. Vertelman, P. J. van Koningsbruggen, M. Knupfer, O. Molodtsova, J.-J. Pireaux, and P. H. M. van Loosdrecht, J. Phys. Chem. C **112**, 14158 (2008).

[15] E. J. M. Vertelman, E. Maccallini, D. Gournis, P. Rudolf, T. Bakas, J. Luzon, R. Broer, A. Pugzlys, T. T. A. Lummen, P. H. M. van Loosdrecht, and P. J. van Koningsbruggen, Chem. Mater. **18**, 1951 (2006).

[16] Y. Nanba and K. Okada, J. Phys. Soc. Jpn. **80**, 074710 (2011).

[17] Y. Moritomo, M. Hanawa, Y. Ohishi, K. Kato, M. Takata, A. Kuriki, E. Nishibori, M. Sakata, S. Ohkoshi, H. Tokoro, and K. Hashimoto, Phys. Rev. B **68**, 144106 (2003).

[18]S. Margadonna, K. Prassides, and A. N. Fitch, Angew. Chem. Int. Ed. **43**, 6316 (2004).
[19]S. Ohkoshi, H. Tokoro, T. Matsuda, H. Takahashi, H. Irie, and K. Hashimoto, Angew. Chem. Int. Ed. **46**, 3238 (2007).
[20]T. Mahfoud, G. Molnár, S. Bonhommeau, S. Cobo, L. Salmon, P. Demont, H. Tokoro, S. Ohkoshi, K. Boukheddaden, and A. Bousseksou, J. Am. Chem. Soc. **131**, 15049 (2009).
[21]S. Ohkoshi, H. Tokoro, and K. Hashimoto, Coord. Chem. Rev. **249**, 1830 (2005).
[22]S. Ohkoshi, T. Matsuda, H. Tokoro, and K. Hashimoto, Chem. Mater. **17**, 81 (2005).
[23]H. Tokoro, T. Matsuda, T. Nuida, Y. Moritomo, K. Ohoyama, E. D. Loutete-Dangui, K. Boukheddaden, and S. Ohkoshi, Chem. Mater. **20**, 423 (2008).
[24]E. D. Loutete-Dangui, E. Codjovi, H. Tokoro, P. R. Dahoo, S. Ohkoshi, and K. Boukheddaden, Phys. Rev. B **78**, 014303 (2008).
[25]R. Fukaya, M. Nakajima, H. Tokoro, S. Ohkoshi, and T. Suemoto, J. Chem. Phys. **131**, 154505 (2009).
[26]A. Asahara, M. Nakajima, R. Fukaya, H. Tokoro, S. Ohkoshi, and T. Suemoto, Phys. Status Solidi B **248**, 491 (2011).
[27]H. Tokoro, K. Nakagawa, K. Imoto, F. Hakoe, and S. Ohkoshi, Chem. Mater. **24**, 1324 (2012).
[28]E. J. M. Vertelman, T. T. A. Lummen, A. Meetsma, M. W. Bouwkamp, G. Molnar, P. H. M. van Loosdrecht, and P. J. van Koningsbruggen, Chem. Mater. **20**, 1236 (2008).
[29]H. Tokoro, S. Miyashita, K. Hashimoto, and S. I. Ohkoshi, Phys. Rev. B **73**, 172415 (2006).
[30]R. Yabuki and K. Nasu, Phys. Lett. A **320**, 286 (2004).
[31]H. Okamoto, Y. Ishige, S. Tanaka, H. Kishida, S. Iwai, and Y. Tokura, Phys. Rev. B **70**, 165202 (2004).
[32]T. Suemoto, K. Ohki, R. Fukaya, M. Nakajima, H. Tokoro, and S. Ohkoshi, J. Lumin. **129**, 1775 (2009).